IBR Power Plant Frequency Control Design Consideration

Lingling Fan, Fellow, IEEE, Zhixin Miao, Senior Member, IEEE, Deepak Ramasubramanian, Senior Member, IEEE

Abstract—Voltage control is often time provided at the plantlevel control of inverter-based resources (IBR). Addition of energy storage systems in an IBR power plant makes it feasible to have frequency control at the power plant level. While frequency control appears as a simple frequency-power droop control to adjust real power commands to inverter-level controls with measured frequency as an input, care must be taken to avoid interactions among the plant frequency control with communication delays, inverter-level control effects, and the frequency sensor, usually a phase-locked-loop (PLL). This paper present two types of interaction scenarios that makes frequency control design challenging. The first interaction scenario may occur if the frequency control's gain is large, while the second interaction scenario may occur at a small control gain if the plant-level PLL lacks sufficient damping. We contribute to the fundamental understanding of the causation of stability issues due to plant frequency control through the derivation of a simplified feedback system focusing on the frequency and power relationship, and the follow-up frequency-domain analysis for gaining insights. For validation, we also design a data-driven approach to obtain models from data generated from an electromagnetic transient (EMT) simulation testbed. The findings from analysis have all been validated by EMT simulation. Finally, we contribute to mitigating strategies and also the understanding of the role of additional proportional integration power feedback control. This addition has been demonstrated as an efficient stability enhancement strategy to mitigate the effect of communication delay.

Index Terms—Solar photovoltaic, phase-locked loop, plant control, frequency control, delay, stability.

I. INTRODUCTION

NVERTER-based resource (IBR) power plants, e.g., solar photovoltaic plus battery energy storage systems, are feasible to provide not only voltage support but also frequency support. While the inverter-level controls are designed by inverter original equipment manufacturers (OEMs), plant-level controls may be designed by a third party. At the plant level, voltage and frequency measurements taken from the Point of Interconnection (POI) bus are used as the input signals for the voltage and frequency controllers. The outputs are usually real and reactive power commands that will be sent to hundreds of inverters through communication systems [1], [2]. This hierarchical control structure is very different from a traditional synchronous generator-based power plant where frequency and voltage controls are all realized at the machine

This project is supported in part by NSF grant 2103480 and in part by EPRI grant. L. Fan and Z. Miao are with the Department of Electrical Engineering, University of South Florida, Tampa, FL, 33620 (e-mail: linglingfan, zmiao@usf.edu). D. Ramasubramanian is with EPRI (email: dramasubramanian@epri.com).

level. In particular, the IBR power plant control design has to consider the impact of communication delay.

Interactions of the plant-level voltage control, the inverter control, and the grid are known to cause oscillatory stability issues. In the 9 August 2019 Great Britain power disturbance, an offshore wind power plant's voltage control led to instability and caused deloading of the power plant [3]. 4-Hz oscillations have been observed in a type-4 wind farm in Texas when the grid strength reduces from short circuit ratio (SCR) at 4 to 2 [4]. 0.1-Hz oscillations have been observed in 1-GW solar PV power plants in California when the real power exporting level reaches a threshold. Mechanism of such instability have been thoroughly examined in [5] and [6] by use of a voltage-reactive power feedback system. A recent report from Grid-India presents many voltage oscillation events caused by plant-level voltage control delay [7]. In short, the plant-level communication delay introduces additional phase lag, thus making the system susceptible to oscillations when the loop gain increases due to the increase of grid impedance, plant-level voltage control gain, or real power exporting level.

On the other hand, few real-world events have been reported to be associated with frequency control except the 19.5-Hz oscillation event occurred in 2021 in an Hawaii Island [8]. Computer simulation experiments have shown that frequency measurement delay, frequency-power droop gain, and PLL's parameters are the influencers of this oscillation mode.

In the literature, few have examined plant-level frequency control and the interaction and coordination of this control with the communication system, the inverter-level control, and the grid characteristics. The current-day books on IBRs, e.g., [9], [10], mainly focus on inverter-level controls. IBR power plant control is not in the scope of these books. Only in a few recent literature, e.g., [1], [2], plant-level frequency control is included in examination. Based on eigenvalue and participation factor analysis, [2] presents the aggregated effect of both voltage and frequency droop control of introducing oscillation modes below 10 Hz. It is desirable to examine the individual influence of frequency control. This is achieved in the authors' research [1]. The interactions of plant frequency control and inverters have been touch based as one of the eight potential operational challenges. It is found that the plant-level frequency control may interact with the communication delay and PLL and create multi-mode oscillations, and weak grid strength worsens instability issues. A feedback system describing the relationship among frequency, power, communication delay, d-axis current, and PLL angle is presented in [1]. This system is shown as a success capable of explaining the cause

1

of the multi-mode oscillations.

The feedback system derived in [1] requires refinement. Additionally, this model needs to be validated against a testbed with detailed circuit dynamics and controls included. Finally, mitigation strategies need to be explored. These gaps have been filled in the current paper. In summary, the goal of the current paper is to evaluate IBR power plant frequency control's impact on system stability and achieve frequency control suitable for weak grid operation. To this end, this paper investigates the potential stability issues due to plant-level frequency-power droop control and how to mitigate them. Not only the simple frequency-power droop control, but also the more sophisticated droop plus PI control are examined. Simulation results that demonstrate the instability phenomena are presented and the mechanism of the interactions is revealed. Compared to our prior work [1] and the existing literature, the contribution of the current paper is three-fold.

- We contribute to the fundamental understanding of the causation of stability issues due to plant frequency control through the derivation of a simplified feedback system focusing on the frequency and power relationship, and the follow-up frequency-domain analysis for gaining insights. Using the simplified model, potential stability issues due to plant-level frequency control have been identified and two types of dynamic phenomena are demonstrated using EMT simulation results of a testbed with circuit dynamics and control details included.
- We also design a data-driven approach to validate the simplified model via comparison against the identified models from data generated from an EMT simulation testbed. The data-driven approach is a worthwhile contribution as it can help engineers aggregate effects from intricate details into a few blocks and further develop a feedback system consisting of a few block diagrams that facilitate analysis.
- Finally, we contribute to stability mitigate strategies and the understanding of the role of additional proportional integration power feedback control. We have demonstrated this addition as an efficient stability enhancement strategy.

In what follows, we present the testbed, analysis and simulation results. The testbed of a multiple-IBR grid integration system is described in Section II. The analytical model, the derivation procedure and the analysis results are presented Section III. As a comparison, the model identified through a data-driven approach, and the analysis results are presented in Section IV. The EMT simulation results demonstrating the two types of interactions are presented in Section V. In Section VI, the more sophisticated control (droop + PI) is analyzed and demonstrated for its impact on stability enhancement. Discussions on plant-level control design consideration are also presented in this section. Section VII concludes this paper.

II. TESTBED

Fig. 1 shows the circuit topology of the system. A 100-MW IBR power plant consisting of a solar PV and a BESS is connected to a 230-kV POI bus. The solar PV represents

the aggregation of many solar PVs and distributed storage systems. Therefore, this solar PV is assumed to have capability to provide frequency control. In the testbed, a single inverter is employed to represent the aggregated solar PV inverters. Another inverter is employed to represent the BESS.

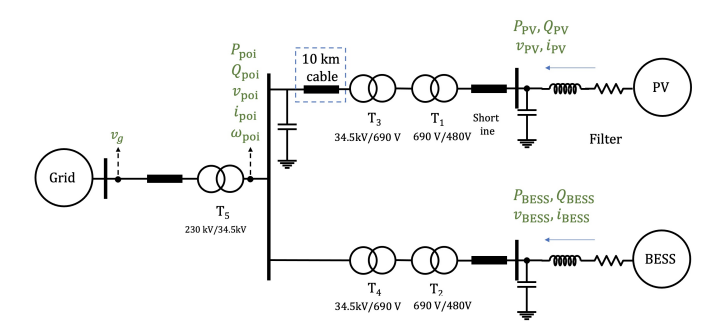


Fig. 1: The circuit topology of a solar plus storage hybrid power plant.

Both IBRs are connected to the POI bus through a choke filter, a short line, and two step-up transformers. The PV system is connected through a 10-km cable to the transformers. The BESS is connected to the POI through a short line and transformers. The entire system has four zones: 480 V, 690 V, 34.5 kV and 230 kV.

Fig. 2 shows the control system of the hybrid power plant. The control system has two levels: the plant level and the inverter level. Both inverters adopt the same grid-following control structure. In Fig. 2, the BESS' inverter-level control details are omitted and replaced by two blocks representing the outer control and the inner control. The inverter-level control regulates real power and reactive power. The plantlevel control has frequency-power droop control and voltage PI control. The plant control center sends out the real power and reactive power commands to the inverter-level control. Communication delay is indicated as e^{-Ts} in Fig. 2. For the inverter-level control, the measurement point is the point of common coupling (PCC) bus. Real power, reactive power, voltage and current at each PCC bus are measured and used in the inverter-level control. The measurement point of the plant-level control is at the POI bus.

The plant-level frequency control has two types, as shown in Fig. 2. The first type is a simple f-P droop control with the frequency as the input and the power command as the output. The second type has an additional power PI feedback control. In addition to the droop control, the power measured at the POI is compared with the power command generated by the droop control and the error is passed to a PI controller. In Sections III-V, the frequency control focuses on the simple f-P droop control. In Section VI, the droop+PI frequency control will be examined.

The parameters of the circuit and controls are listed in Tables I and II.

This testbed has been built in MATLAB/Simscape specialized power systems environment to provide EMT simulation results. To speed up the computing speed, the two inverters are represented by average models with power electronics switching details ignored.

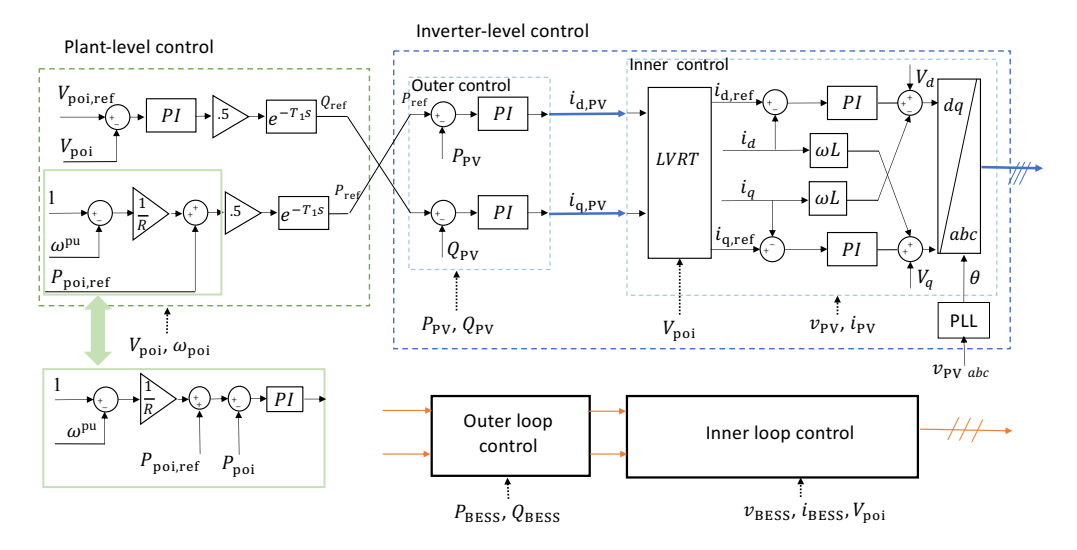


Fig. 2: The control system of the HPP consists of the plant-level control and the inverter-level control. Frequency control at the plant can be a simple f-P droop control or a droop + PI control.

TABLE I: Parameters of the electric system.

Description	Item	Values
Rated Power	S_{base}	100 MW
Inverter terminal voltage	V_p	480 V
Inverter transformer voltage	$\dot{V_s}$	690 V
Medium voltage	$V_{\rm POI}$	34.5 kV
High voltage	V_g	230 kV
Nominal frequency	ω_0	377 rad/s
Filter (RL)	$Z_{ m RL}$	0.003 + j0.15 pu
Filter (C)	Q_C	0.01 pu
Short line impedance	Z_s	0.01 + j0.1 pu
Transformer impedance	Z_T	0.003 + j0.06 pu
10-km 34.5 kV cable impedance	Z_c	0.16 + 0.286 p.u.
Shunt capacitor	$Q_{ m SVD}$	0.1 p.u.
Grid line impedance	Z_g	0.028 + j0.28 p.u.

TABLE II: Parameters of the plant and inverter-level controls.

Description	Item	Values	Bandwidth
Current control	PI	1 + 10/s p.u.	400 Hz
Ral power control	PΙ	0.25 + 25/s p.u.	3.3 Hz
Reactive power control	PΙ	0.4 + 40/s p.u.	5 Hz
Plant-level f-P droop	R	1 - 5%	n.a.
Plant-level frequency	PΙ	0.1 + 1/s	0.1 Hz
Plant-level voltage control	PΙ	0.1 + 7/s p.u.	1 Hz
Inverter-level PLL	PΙ	60 + 1400/s p.u.	13 Hz
Plant-level PLL	PΙ	20 + 200/s p.u.	4.6 Hz
Delay	T	50 ms to 100 ms	n.a.

III. ANALYSIS BASED ON A SIMPLIFIED FEEDBACK SYSTEM

To examine the interaction of the plant frequency control with the rest of the system, we seek a linear feedback system. In Sections III and IV, we present analysis results based on two types of models. The first is based on a simplified feedback system model from first principle; while the second is based on a data-driven model obtained from the EMT testbed which includes all details. The objective of the simplified model is to focus on the frequency-real power relationship while omitting the effect of reactive power/voltage and associated control. Such simplification can help revealing the potential

stability issues associated with frequency and real power. For validation, we rely on system identification technology to identify an input/output model describing the frequency and real power relationship. The model derived from the first principle will be compared from the model identified from data in Section IV.

A. Derivation of a simplified feedback system

The simplified feedback system consists of the effect of the plant-level frequency control, the communication delay, the inverter-level real power control, the grid imedance, and the PLL at the POI. For simplification, this feedback system is based on the assumption of a single inverter representing the entire IBR power plant as a controllable current source. The PCC bus and the POI bus are assumed to be the same. The grid is represented by a constant voltage source behind a pure reactance. The transmission grid EMT dynamics and fast inner control dynamics have all been ignored. However, the inverterlevel PLL and the POI PLL for plant-level frequency control are differentiated. They have very different functions as the inverter-level PLL is used for synchronization while the plantlevel POI PLL is used for sensing frequency measurement only. Due to their different purposes, the two types of PLLs may have different parameters and different bandwidths.

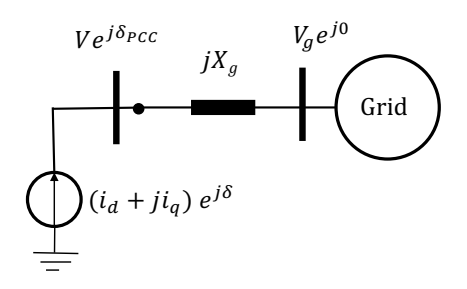


Fig. 3: The equivalent circuit.

The circuit topology of the assumed system is shown in Fig. 3. The inverter is viewed as a controllable current source

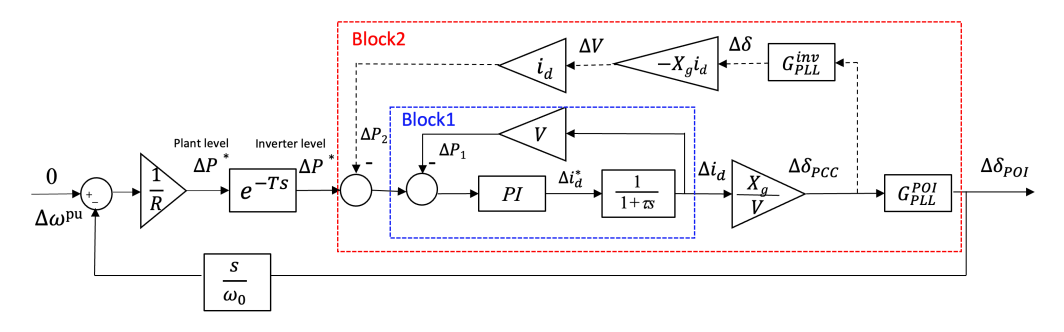


Fig. 4: The frequency-power feedback system consisting of plant-level frequency control, delay, d-axis outer control and PLL. Block2 has the inverter level power order as the input and the plant-level PLL's angle as the output. This block is also identified in Section IV using a data-driven approach.

 $(i_d+ji_q)e^{j\delta}$, where i_d and i_q are the inverter PLL frame's dq current injection and δ is the inverter-level PLL's angle. The grid voltage is assumed as a constant voltage source and the grid impedance is jX_g . The current source influences the PCC bus' voltage phasor $Ve^{j\delta_{\rm PCC}}$, where $\delta_{\rm PCC}$ is the phase angle and the PLL's angle δ tracks $\delta_{\rm PCC}$.

The effect of the inner current control effect is simplified as a low-pass filter $1/(1+\tau s)$. A part of the feedback system, from the inverter-level power command ΔP^* to a PLL's output angle, has been derived in [11]. In this paper, the full feedback system consisting of plant control will be derived. In the following, the derivation procedure is rigorously presented to illustrate the mathematical reasoning.

It is perceivable that the plant-level frequency control uses frequency sensed by the PLL at the POI as the input while generates power command. The power command will be sent to the inverter, which influences the angle of the inverter bus $\delta_{\rm PCC}$. Hence, it is necessary to characterize the system from the inverter-level power command to the POI's PLL angle $\delta_{\rm POI}$.

Prior research in [11] has shown that a PLL's output angle tries to track the input PCC voltage's angle. The transfer function between the output angle and the input PCC voltage angle $\delta_{\rm PCC}$ is the closed-loop PLL transfer function. Therefore:

$$\frac{\Delta \delta_{\text{POI}}}{\Delta \delta_{\text{PCC}}} = G_{\text{PLL}}^{\text{POI}}, \ \frac{\Delta \delta}{\Delta \delta_{\text{PCC}}} = G_{\text{PLL}}^{\text{inv}}. \tag{1}$$

Next, we may use the circuit in Fig. 3 to find the relationship between δ_{PCC} and the current injection $(i_d + ji_q)e^{j\delta}$. It has to be emphasized that the δ is the inverter-level PLL's angle.

Assume that the grid impedance is represented by a pure reactance and the EMT dynamics of the grid are ignored. Then the PCC bus voltage phasor is related to the current injection as follows.

$$Ve^{j\delta_{PCC}} = V_g + jX(i_d + ji_q)e^{j\delta},$$
 (2)

The above equation is linearized by considering i_d , i_q , δ 's variation. The grid voltage V_g is assumed to be constant. Hence,

$$\Delta(Ve^{j\delta_{\text{PCC}}}) = e^{j\delta_{\text{PCC}}}\Delta V + jVe^{j\delta_{\text{PCC}}}\Delta\delta_{\text{PCC}},$$

= $jX_g(\Delta i_d + j\Delta i_q)e^{j\delta} - X_g(i_d + ji_q)e^{j\delta}\Delta\delta.$ (3)

At the initial steady-state condition, $\delta_{PCC} = \delta$. Hence the above equation becomes:

$$\Delta V = -X_g i_d \Delta \delta - X_g \Delta i_q, \tag{4}$$

$$\Delta \delta_{\text{PCC}} = \frac{X_g}{V} \Delta i_d - \frac{X_g i_q}{V} \Delta \delta. \tag{5}$$

Eqs. (4) and (5) will be simplified by ignoring the effect of voltage and reactive power control, as well as the effect of steady-state reactive power: $\Delta i_q \approx 0$ and $i_q \approx 0$. This omission leads to (6) and (7).

$$\Delta V = -X_q i_d \Delta \delta, \tag{6}$$

$$\Delta \delta_{\text{PCC}} = \frac{X_g}{V} \Delta i_d. \tag{7}$$

This omission is reasonable with the aim of deriving a simplified model focusing on frequency and real power relationship. Nevertheless, the derived simplified model will be compared with the model identified from experiment data based on the EMT testbed. In that testbed, the voltage and reactive power control is in place and the reactive power is not zero.

It can be seen that i_d directly influences the PCC bus angle $\delta_{\rm PCC}$. This influence becomes more significant if X_g is large or the grid becomes weak. It is necessary to characterize the relationship between the inverter-level power command P^* and i_d . It is known that in the PLL frame:

$$P = Vi_d. (8)$$

Therefore,

$$\Delta P = \underbrace{V\Delta i_d}_{\Delta P_1} + \underbrace{i_d \Delta V}_{\Delta P_2}.$$
 (9)

If ΔP_2 , or the effect of ΔV on ΔP is ignored, i.e., the grid is very strong and the voltage of the PCC bus is almost constant, then the inverter's real power ΔP is influenced by Δi_d only:

$$\Delta P \approx \Delta P_1 = V \Delta i_d. \tag{10}$$

The inner current control enforces current tracking. In the simplified model, the transfer function from the inner current order i_d^* generated by the real power control to the measurement i_d is simplified as

$$\frac{\Delta i_d}{\Delta i_d^*} = \frac{1}{1 + \tau s},\tag{11}$$

where $\tau = 0.01$ s.

With the outer power control, we may find the transfer function from P^* to i_d as the following.

$$\frac{\Delta i_d}{\Delta P^*} = \underbrace{\frac{\left(K_p + \frac{K_i}{s}\right)\frac{1}{1+\tau s}}{1+V\left(K_p + \frac{K_i}{s}\right)\frac{1}{1+\tau s}}}_{G_{\text{Plock!}}} \tag{12}$$

Based on above relationship of P^* , i_d , δ_{PCC} , δ , δ_{POI} , and V, along with the plant-level control, a feedback system is assembled and presented in Fig. 4.

B. Analysis

Block1 in Fig. 4 is essentially a low-pass filter. Since the bandwidth of the power control (3.3 Hz), we may use a low-pass filter with a time constant 0.05 s to represent Block 1.

$$G_{\text{Block1}} = \frac{\left(0.25 + \frac{25}{s}\right) \frac{1}{1 + 0.01s}}{1 + V\left(0.25 + \frac{25}{s}\right) \frac{1}{1 + 0.01s}} \approx \frac{1}{1 + 0.05s}.$$
 (13)

Fig. 5 shows the comparison of the frequency responses of the second-order model vs. the first-order model for Block1. They have very similar responses.

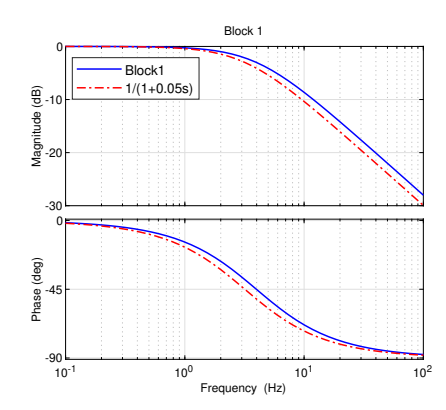


Fig. 5: Comparison of G_{Block1} vs. $\frac{1}{1+0.05s}$.

If ΔP_2 is ignored, the transfer function from the inverterlevel ΔP^* to the POI's PLL angle $\Delta \delta_{\rm POI}$ is

$$\frac{\Delta \delta_{\text{POI}}}{\Delta P^*} = \frac{X_g}{V} \cdot G_{\text{Block1}} \cdot G_{\text{PLL}}^{\text{POI}}.$$
 (14)

Otherwise, the transfer function is expressed as

$$\frac{\Delta \delta_{\text{POI}}}{\Delta P^*} = \frac{\frac{X_g}{V} \cdot G_{\text{Block1}}}{1 - X_g i_d^2 \frac{X_g}{V} G_{\text{PLL}}^{\text{inv}} \cdot G_{\text{Block1}}} G_{\text{PLL}}^{\text{POI}}.$$
 (15)

Fig. 6 shows the comparison of the frequency responses of $\frac{\Delta\delta_{\rm POI}}{\Delta P^*}$ with or without consideration of ΔP_2 or the voltage feedback effect under two grid conditions: X_g at 0.2 pu vs X_g at 0.5 pu. It can be seen that when X_g is 0.2 pu or under relatively strong grid strength condition, the effect of ΔP_2 is negligible. On the other hand, when X_g is 0.5 pu or the grid is weak, ΔP_2 or the feedback effect of V mainly influence the magnitude for the below 2 Hz region. Fig. 6 clearly shows that a weaker grid leads to a higher gain in all frequency region. Therefore, it is projected that transmission line tripping events may lead to potential risk of instability.

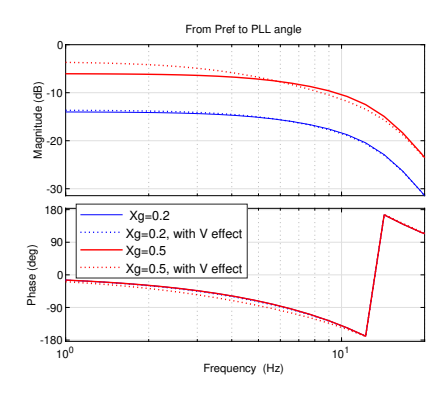


Fig. 6: Comparison of the transfer function $\frac{\Delta \delta_{\rm POI}}{\Delta P^*}$ with or without consideration of ΔP_2 or the voltage feedback effect for two grid conditions. Both PLLs have PI controller parameters as (60, 1400).

For the system under study, when the grid strength viewed from the POI bus is relatively strong, e.g., when the grid impedance is 0.2 pu, in the analytical model, the effect of ΔP_2 may be ignored. Thus, according to the block diagram in Fig. 4, the final loop gain including the plant-level control and inverter-level control has the following expression.

Loop Gain =
$$\frac{1}{R\omega_0}e^{-Ts}\frac{1}{1+0.05s}\frac{X_g}{V}G_{\rm PLL}^{\rm POI}s$$

= $ke^{-0.05s}\frac{1}{1+0.05s}0.2\ G_{\rm PLL}^{\rm POI}\ s$ (16)

where $k = 1/(R\omega_0)$ pu/(rad/s).

Remark: Based on the loop gain, it is clear to see that the plant-level control may interact with the plant-level PLL. Specifically, the plant-level delay introduces additional phase lag. If the grid is weak or the plant-level frequency control gain is too large, oscillatory instability may be induced.

In the following, the effect of the plant-level control gain and the PLL will be examined. The linear system block diagram of a PLL is shown in Fig. 7.

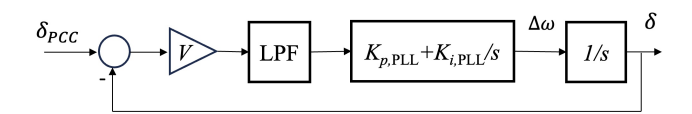


Fig. 7: The closed-loop system of a PLL that tracks the PCC bus voltage phase angle $\delta_{\rm PCC}$ while outputs a measured angle δ .

PLL1 has its PI parameters as (60, 1400) while PLL2 has its PI parameters as (120, 2000). Both PLLs have a second-order low-pass filter with a cutoff frequency at 25 Hz employed. The inclusion of the low-pass filter is necessary since majority of PLLs have the unit to smooth the input signal. Ref. [12] conducted frequency scan experiments and has verified that a synchronous reference frame-based second-order PLL with the inclusion of a filter has the same frequency response as the three-phase PLL used in the MATLAB/Simscape Specialized Power System library. The closed-loop system of the PLL is

as follows.

$$G_{\text{PLL}} = \frac{G_{\text{LPF}}\left(K_{p,\text{PLL}} + \frac{K_{i,\text{PLL}}}{s}\right) \frac{1}{s}}{1 + G_{\text{LPF}}\left(K_{p,\text{PLL}} + \frac{K_{i,\text{PLL}}}{s}\right) \frac{1}{s}}$$
(17)

where

$$G_{\mathrm{LPF}} = \frac{\omega_f^2}{s^2 + 2\zeta\omega_f s + \omega_f^2},$$

and $\omega_f = 2\pi \times 25$ rad/s and $\zeta = 0.707$.

For the two PLLs, the closed-loop system frequency responses are shown in Fig. 8a. It can be seen clearly that PLL2 lacks damping and its magnitude shows a peak of 10 dB at 20 Hz.

Fig. 8b presents the Bode diagrams of the loop gain for three sets of parameters. It can be seen that there are two conditions that oscillatory instability can occur.

- 1) f-P control gain is large;
- 2) PLL lacks damping.

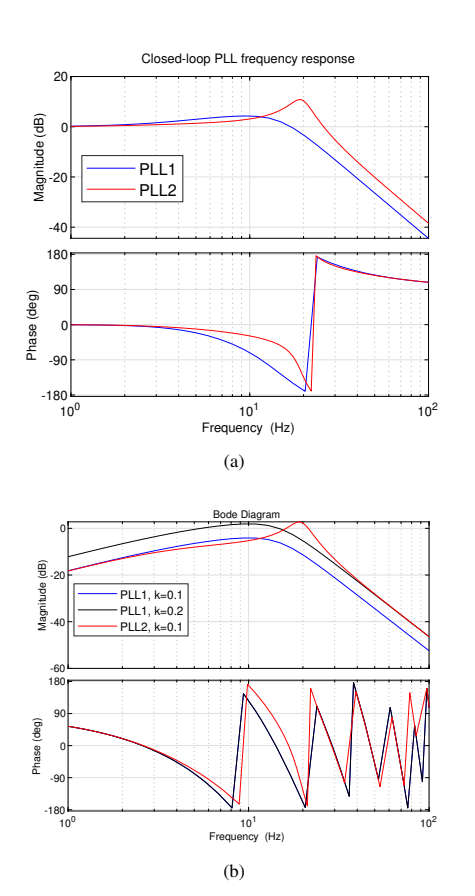


Fig. 8: (a) Comparison of two PLLs. (b) The loop gain of the frequency feedback system.

1) Large f-P control gain: First, if the f-P control gain in the plant level is too large, instability may occur. In this numerical example, when k=0.2 pu/(rad/s), the gain margin at the phase shifting frequency at about 8 Hz is negative. Note that k=0.2 pu/(rad/s) is equivalent to a P-f droop parameter of 5/377 or 1.33%. k=0.1 pu/rad/s is equivalent to a P-f droop gain of 2.65% In another word, the P-f droop R cannot be too small.

This instability has much to do with the combined effect of the communication delay and the f-P proportional gain. At 10 Hz, 50 ms delay introduces 180 degrees phase lag. A larger delay of 100 ms introduces 180 degrees phase lag at 5 Hz. Fig. 9(a) shows the loop gain under different communication delay time when k = 0.2 pu/(rad/s) and PLL1 is adopted. It can be seen that the loop gain's magnitude is greater than 0 dB in the frequency range of 5 Hz - 15 Hz. Therefore, for a delay of 50 ms to 100 ms, a large f-P gain is an issue. The delay time influences the oscillation frequency. When the delay is 50 ms, the phase shifting occurs at 8 Hz. When the delay is 100 ms, the phase shifting occurs at 5 Hz and 12 Hz. Fig. 9(b) shows the closed-loop linear system's step responses subject to different delay. The time-domain simulation results confirm the Bode diagram-based stability analysis and show that the system is subject to 8-Hz oscillations when the delay is 50 ms and subject to 5-Hz and 12-Hz oscillations when the delay is 100 ms.

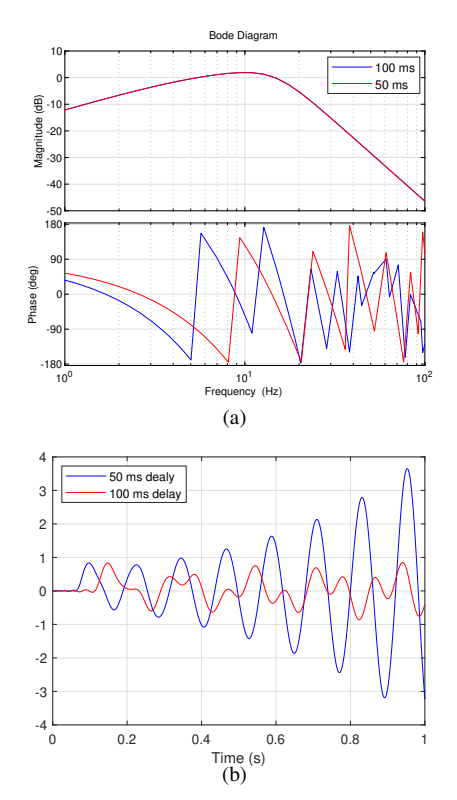


Fig. 9: (a) Frequency response of the loop gain when $k=0.2~\rm pu/(rad/s)$ and PLL1 is adopted. For both cases (50 ms or 100 ms delay), the system is unstable. For the 50 ms delay case, the phase shifting occurs at 8 Hz, implicating 8-Hz oscillations. For the 100 ms delay case, the phase shifting occurs at 5 Hz and 12 Hz, implicating multi-mode oscillations. (b) Step responses of the closed-loop system.

2) PLL lacking damping: In the second instability scenario of PLL lacking damping, the f-P gain is small (k=0.1 pu/(rad/s)). Based on the comparison shown in Fig. 8b, it can be seen that when PLL1 is replaced by PLL2, the loop gain's magnitude has a peak over 0 dB at 20 Hz. At 20 Hz, the phase is less than -180 degrees. Therefore, this condition may cause 20-Hz oscillations. This issue is caused by the plant-level PLL predominantly. Therefore, a plant-level PLL is required to have

sufficient damping.

The findings from the above analysis align with the findings from the computer simulation for the 19.5-Hz oscillation [8]. According to [8], reducing the f-P control gain (or increasing the P-f droop gain), reducing PLL's gain, reducing grid impedance, and reducing delay all help mitigate oscillations. The root cause has been summarized as "GFLs with larger frequency measurement-delays and non-optimal parameterization operating under weak grid conditions." [8]. All these four measures reduce the overall loop gain or phase lag of the feedback system presented in Fig. 4. In turn, stability can be enhanced. The frequency-power feedback system indeed sheds insights on this real-world event.

IV. ANALYSIS BASED ON A DATA-DRIVEN MODEL

The frequency responses in the previous subsection are based on a simplified feedback system. In this subsection, we present the analysis results based on the model obtained from experiment data of the EMT testbed. In order to conduct sensitivity analysis on delay and droop gain, a subsystem will be identified from data. This subsystem is Block2, highlighted in Fig. 4.

To identify this subsystem, in the EMT testbed, the frequency-power droop control in the plant level is first disabled. A step change in the real power command of the inverter control surely causes an increase in the PLL angle at steady state. This characteristics indicates that the system of the PLL angle vs. the real power command is similar to a low-pass filter. This system will be identified using step response data. The real power command at the solar inverter control level is perturbed and the PLL angle measured based on the POI bus voltage are recorded. Based on this set of the data, the input/output transfer function from the power command to the PLL angle δ_{POI} is obtained by use of system identification algorithms. Relying on this transfer function, the communication delay, and the f-P droop control, the loop gain of the entire f-P feedback system is obtained and stability analysis can be conducted.

Fig. 10(a) shows the input and the output data that will be used to identify the transfer function $\frac{\Delta \delta_{\text{POI}}}{\Delta P^*}$. PLL1 or PLL2 is used in the EMT testbed to generate data. It can be seen that when PLL2 is adopted, the output data of y1 have apparent ripples in the otherwise smooth response. System identification requires the balance between bias and variance [13]. A high-order model reduces bias. However, introducing many more parameters increases variance. Therefore, picking a suitable order is necessary and this is done by examining the matching degree of the model output and the measured output for different model order assumptions. For this study, the model order of 4 leads to the excellent matching degree. Therefore, a 4th order transfer function is identified using MATLAB System Identification Toolbox's tfest. The step responses from the two identified models are compared in Fig. 11. It can be seen that high matching degree has been achieved.

Fig. 10(b) shows the frequency responses of the identified models when PLL1 or PLL2 is used. It can be seen that

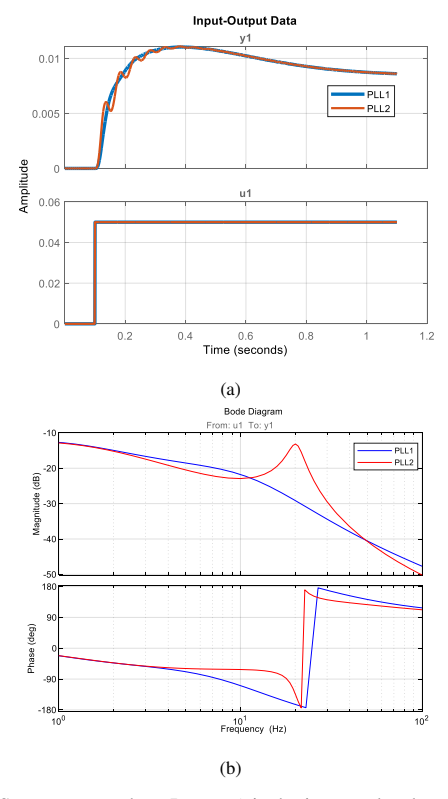


Fig. 10: (a) Step response data. Input u1 is the inverter-level power command while output y1 is the POI PLL's phase angle. (b) Frequency responses of the identified models describing the input and output relationship of PLL angle vs. the inverter power command.

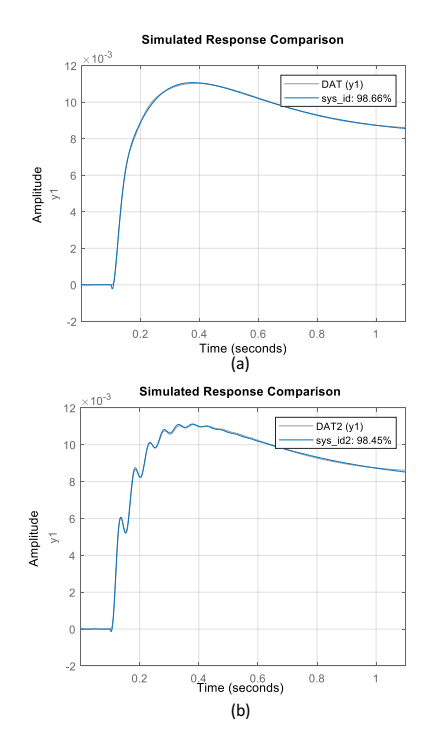


Fig. 11: Comparison of the simulated responses vs. the measurement data. (a) PLL1. (b) PLL2.

different PLL causes a significant difference in the 20 Hz frequency range. PLL2 introduces a peak at 20 Hz.

In addition, Fig. 12 shows the comparison of the identified models vs. the analytical models derived in Section III. It can be seen that the analytical model based on simplified assumptions can capture the frequency responses in the low frequency region. If PLL1 is employed, the matching between the analytical model vs. the identified model is acceptable for the region below 13 Hz. If PLL2 is employed, the matching is acceptable for the region below 30 Hz.

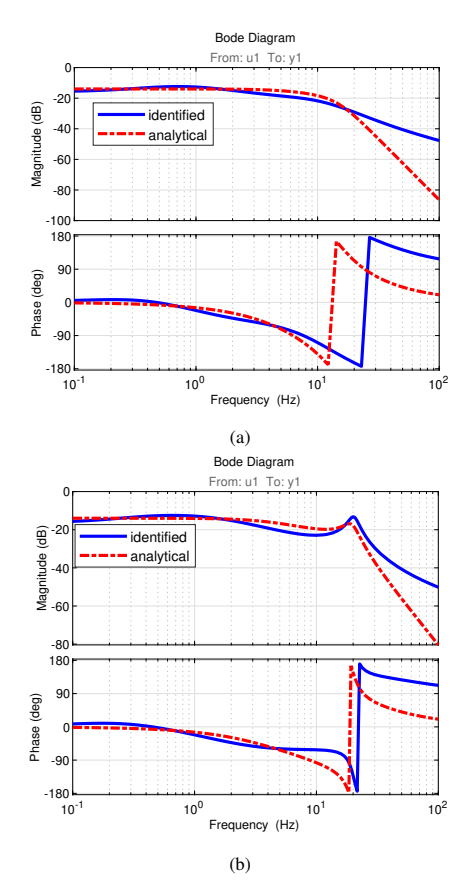


Fig. 12: Comparison of frequency responses of the identified models vs the analytical models when different PLLs are used. (a) PLL1. (b) PLL2.

Finally, the loop gain can be found based on the identified transfer function for $\frac{\Delta \delta_{\rm POI}}{\Delta P^*}.$

Loop Gain =
$$k \cdot e^{-Ts} \cdot \frac{\Delta \delta_{\text{POI}}}{\Delta P^*} \cdot s$$
 (18)

Fig. 13 shows loop gains for different f-P gain, communication delay, and PLL. Again, the two types of instability can be predicted based on the loop gain. When the f-P gain is large (at 0.2 pu/(rad/s)), oscillations below 10 Hz may occur even the PLL has sufficient damping. When the PLL2 is adopted, even when the f-P gain is small, oscillations at 20-Hz will be seen. Even with only 10 ms delay, phase shifting will occur at 20 Hz, which again leads to 20-Hz ripples.

The findings based on the data-driven model again show that there exist two types of oscillation phenomena, either due to a large f-P gain or PLL lacking damping.

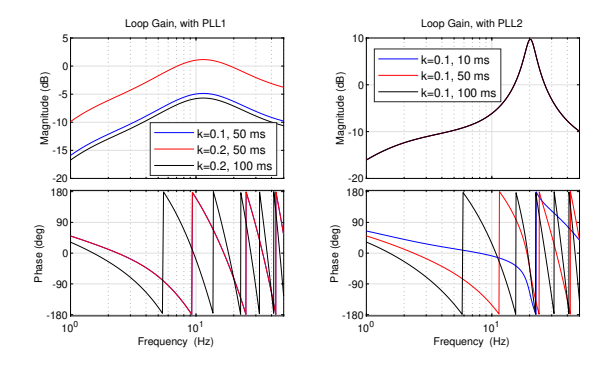


Fig. 13: Frequency responses of the loop gain based on the identified model. Bode diagrams in the left column show large f-P gain may cause instability and Bode diagrams in the the right column show PLL lacking damping may cause instability.

V. EMT SIMULATION RESULTS

The above analysis results will be verified by the EMT simulation results. A grid line tripping event is assumed and the eventually the grid impedance viewed from the 220-kV POI bus is 0.2 pu. Fig. 14 shows the simulation results when PLL1 is adopted. The plots show the measured real and reactive power at the solar PV terminal, BESS terminal, the POI bus, along with the power commands, and the angles and magnitudes at the solar PV, BESS and the POI bus. Comparison is made to examine the effect of f-P control gain and the delay. It can be seen in Fig. 14(a) that when the f-P gain is 0.1 pu/(rad/s) and the delay is 50 ms, the system is stable. For the same delay, when the f-P gain is 0.2 pu/(rad/s), after line tripping, oscillations at about 7 Hz appear as shown in Fig. 14(b). If the delay is 100 ms, and the f-P gain is 0.2 pu/(rad/s), the line tripping event introduces oscillations of multiple modes, as shown in Fig. 14(c). Visual examination shows that there are 4-Hz and 12-Hz oscillations.

For the testbed with PLL2, the simulation results are shown in Fig. 15. The f-P gain is 0.1 pu/(rad/s) for all the cases. Three communication delays are examined. Fig. 15(a) shows the effect when 10 ms delay is used. Fig. 15(b) shows the effect when 50 ms delay is used, and Fig. 15(c) shows the effect when 100 ms delay is used. It can be seen that 20-Hz ripples become obvious when delay is 50 ms and 100 ms.

Comparing the simulation results in Fig. 14 and Fig. 15, it can be seen that if the oscillations are due to PLL's insufficient damping only, the ripples in the voltage, real power and reactive power measurements are limited to a few percents of the nominal values. 50 ms delay vs. 100 ms delay makes no difference. On the other hand, if the oscillations are due to large f-P gain, oscillations have a peak-to-peak size of 50% in the real power measurement, 20 degrees in the angle measurements, and 20% in the voltage magnitudes.

The EMT simulation results have demonstrated two types of instability caused by the interactions of the plant-level frequency control and the rest of the system due to either a large f-P gain or PLL with insufficient damping.

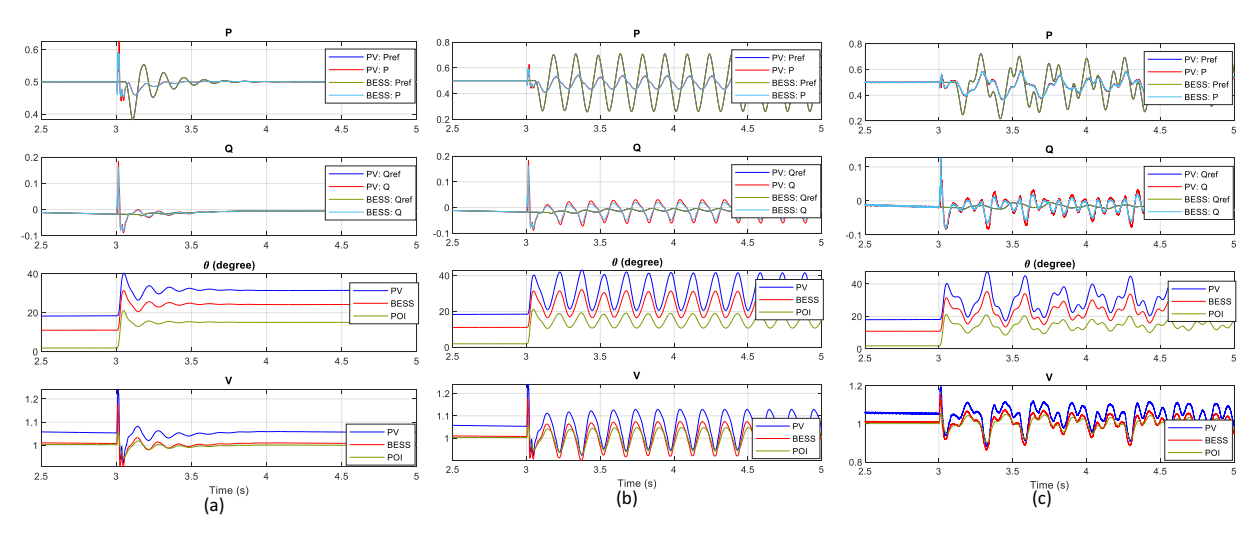


Fig. 14: EMT simulation results for a line tripping event leading to SCR of 0.2 when PLL1 is implemented. (a) k = 0.1 pu/(rad/s), 50 ms delay. (b) k = 0.2 pu/(rad/s), 50 ms delay. (c) k = 0.2 pu/(rad/s), 100 ms delay.

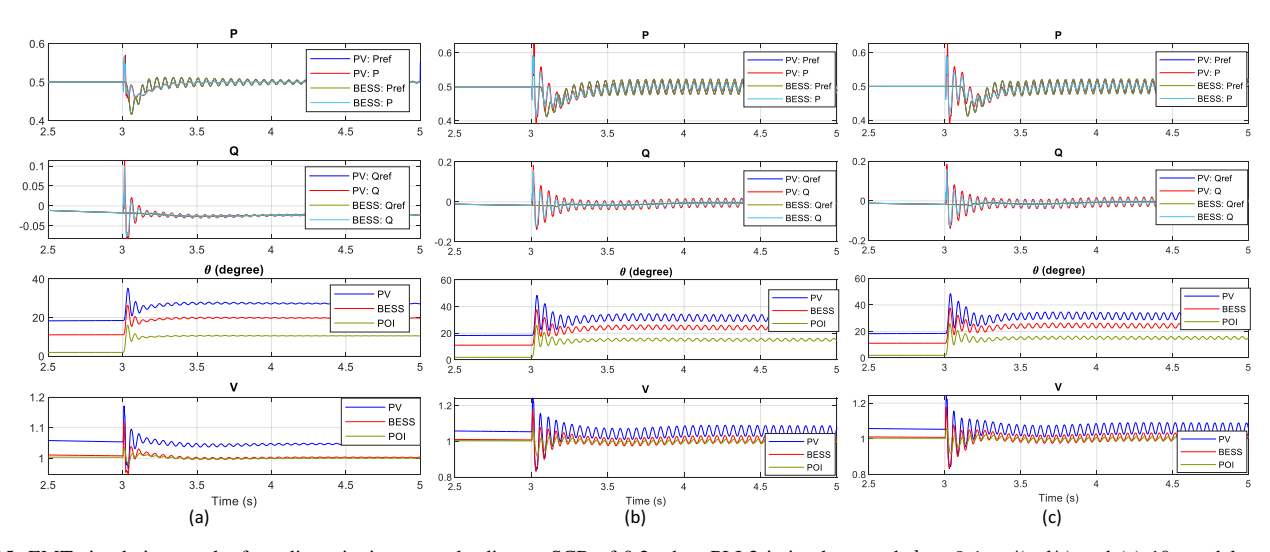


Fig. 15: EMT simulation results for a line tripping event leading to SCR of 0.2 when PLL2 is implemented. k = 0.1 pu/(rad/s) and (a) 10 ms delay; (b) 50 ms delay; and (c) 100 ms delay.

VI. STABILITY ENHANCEMENT STRATEGIES

A. Strategy 1: Slower PLL

The above studies show that caution should be taken on the POI PLL. The previous studies have shown that when the droop parameter R is selected to be 1.33%, the corresponding f-P gain is 0.2 pu/(rad/s). At this condition, even at a strong grid ($X_g=0.2$, SCR at 5), the system is subject to oscillations when a typical PLL is adopted.

While a PLL's closed-loop transfer function is in general a low-pass filter, it can be seen that a smaller gain in the 1 Hz - 20 Hz region is preferred. Thus, a slower PLL is examined for stability improvement. In the following, the PLL at the POI is tuned to have (20,200) as its PI parameters. Fig. 16 shows the comparison of the loop gain when $X_g=0.2$ pu for two PLLs. It can be seen that the slower PLL leads to a stable system, while PLL1 leads to oscillations.

Fig. 17 shows the EMT simulation results for a line tripping event (X_q increases from 0.2 pu to 0.5 pu) when the slow PLL

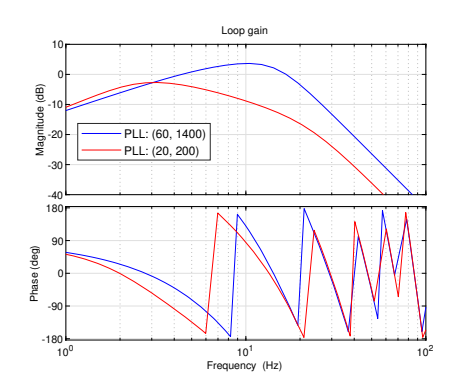


Fig. 16: Frequency responses of the loop gain for two types of PLL. The slower PLL leads to a stable system when the f-P gain k=0.2 pu/(rad/s) and $X_g=0.2$ pu.

is deployed at the plant control. For the inverter-level, PLL1 with (60, 1400) parameters continue to be used. It can be seen

that a slower PLL for the plant frequency control can improve operation and the system's marginal condition improves (SCR at 2) when a large f-P gain (k = 0.2 pu/(rad/s)) is adopted.

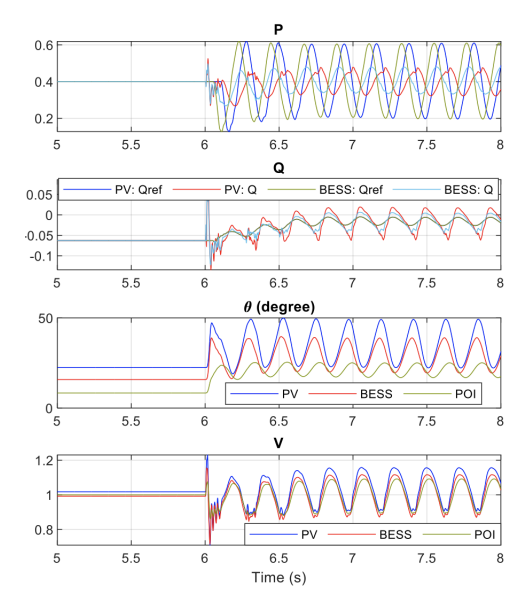


Fig. 17: EMT simulation results for a line tripping event at $t=6\,\mathrm{s}$. X_g changes from 0.2 pu to 0.5 pu; and the system shows 4-Hz oscillations. The communication delays to the PV and BESS are 100 ms and 50 ms respectively.

While the slower PLL has helped improve stability, the system is still subject to oscillations at SCR of 2. Is there a more efficient way to improve stability? In the subsection below, the f-P droop + PI control is examined.

B. Strategy 2: Additional power PI feedback control

We first use a simplified diagram to examine the effect of the PI power feedback control. Fig. 18 presents the revised feedback system. For simplicity, ΔP_2 , or the influence of ΔV on ΔP has been ignored. Thus, in the diagram the inverter-level power command to i_d is simplified by a low-pass filter Block1. For the plant-level power feedback, the effect of ΔV on ΔP is again ignored. Hence, the feedback is same to have Δi_d tied back. The dotted line and the block are the additions when the power PI feedback control is introduced.

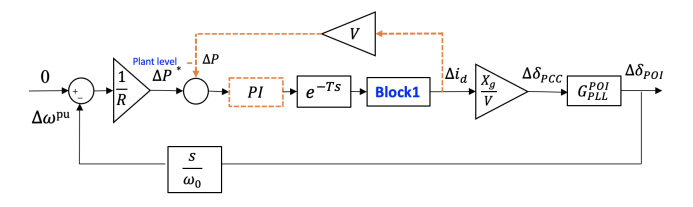


Fig. 18: Frequency-power feedback system diagram considering the f-P droop +PI control.

We now examine the transfer function from the plant-level power command ΔP^* to the inverter PLL frame's Δi_d . Two scenarios of the plant frequency control are compared: f-P droop only and with the addition PI power control. Fig. 19 shows that the PI control with parameters of (0.1, 1) or (0.3, 1) significantly reduces the magnitude of the transfer function

from 1-20 Hz by 20 dB or 10 dB. On the other hand, the phase lag introduced by the PI feedback control is not significant. This shows that the power PI control can effectively reduce the influence of the delay through attenuation.

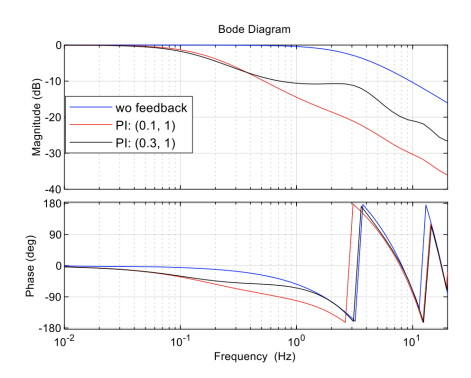


Fig. 19: Frequency responses of $\frac{\Delta i_d}{\Delta P^*}$. It can be seen that the PI control reduces the magnitude.

Fig. 20 shows the EMT simulation results that demonstrate the effect of the PI control. In the beginning, the frequency control has droop control only and the droop parameter R is 1.33% (or k=0.2 pu/(rad/s)). At t=6, a line tripping event occurs and X_g increases from 0.2 pu to 0.5 pu. Oscillations appear. At t=8 s, the additional PI control with (0.3, 1) parameters is enabled. The oscillations are suppressed. Additional experiments show that with the addition of power PI feedback control, the droop control's gain can be increased to 0.6 pu/(rad/s) until oscillations appear. If the droop gain is kept at 0.2 pu/(rad/s), the system has no stability issue introduced due to plant frequency control for very weak grid conditions.

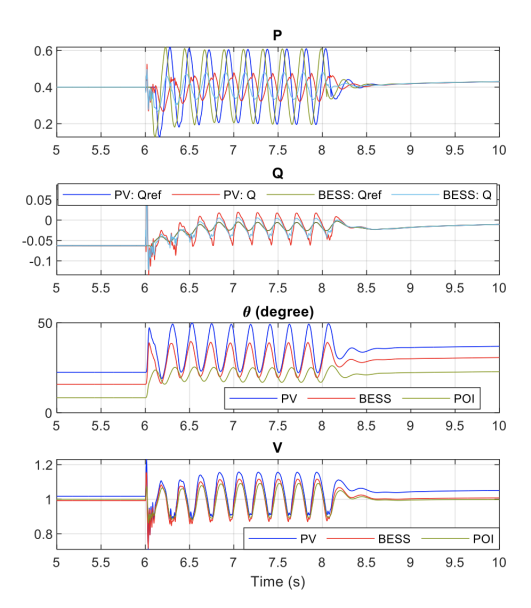


Fig. 20: EMT simulation results for a line tripping event at $t=6\,$ s. X_g changes from 0.2 pu to 0.5 pu; and the system shows 4-Hz oscillations. At $t=8\,$ s, the power PI control is enabled. Oscillations are mitigated.

This set of analysis reveals the mechanism of how the additional power PI unit in the plant frequency control can enhance oscillation stability. The EMT simulation results further verify

and demonstrate the effect of the additional PI power feedback unit.

C. Discussions: Plant-level control design consideration

For the plant-level frequency control design, it can be seen that caution should be taken. The frequency-power feedback system derived in the paper shows that weak grid, large f-P droop control gain, and large PLL transfer function magnitude, can all contribute to the overall loop gain magnitude. Combining the phase lag introduced by the communication delay, a large overall loop gain may introduce oscillations.

To avoid such instability issues, plant-level PLLs with slower responses are preferred. In addition, its closed-loop transfer function depicting the frequency response of angle tracking should not have large peaks at any frequency region. Furthermore, the droop + power PI feedback control is preferred. These measures reduce the overall loop gain magnitudes in the relevant frequency region and lead to a feasible frequency control design for IBR power plants.

For stability check, the linear block diagram shown in this paper offers a quick check for the given communication delay. For better accuracy, parts of the block diagram related to inverter performance may be found through data-driven methods.

D. Discussions: Grid-Forming Control

According to the report from the grid industry [14], there are four types of IBRs:

- legacy IBRs which inject active power at unity power factor and provide no grid support services,
- conventional IBRs which have capability to provide both frequency and voltage responses typically at a plant level with full delivery over multiple seconds,
- enhanced IBRs which can provide full frequency and voltage responses within 1s of event and can survive loss of synchronous machines, and
- future IBRs which are capable of balckstart and could potentially single handedly survive extreme events.

Most IBRs are legacy IBRs of GFL type. Few IBRs are conventional IBRs. Very few IBRs are enhanced IBRs and future IBRs is an area of active research. The IBRs discussed in this paper are indeed conventional IBRs that can provide frequency and voltage support through plant-level control. Many legacy IBRs can be improved to have such capability and this paper shows the potential stability risks and provides a guideline of plant-level control design.

Grid-forming (GFM) control has been proposed to provide fast frequency and voltage support. In US, there are a few pilot projects ongoing. Compared to a GFL where a PLL is used as a synchronizing unit, GFM may use power-based synchronization to provide a synchronizing angle. Therefore, in GFM, P-f droop control is implemented in the inverter level and the delay effect can be ignored. If the plant-level control adopts open-loop control to send the power command to inverters, the plant-level control will not interact with the inverter-level control. Hence, the type of oscillations presented in this paper

may not be seen. In the 19.5-Hz oscillation case [8], when the GFL IBRs are replaced by GFM IBRs, the oscillations no longer appeared. On the other hand, coordination among parallel GFM-IBRs is necessary to avoid interactions or inter-IBR oscillations. This type of interactions has been reported in the literature, e.g., [15], [16].

VII. CONCLUSION

This paper examines the potential stability risks when the plant-level frequency control is introduced for an IBR power plant. The plant-level frequency control introduces coupling of frequency and power. A simplified analytical model describing the frequency power feedback system is derived in this paper for quantitative analysis. Analysis based on this model leads to the findings of two distinct instability phenomena, one due to large f-P gain and one due to insufficient PLL damping. Neither phenomena have been identified in the literature. To confirm our findings, an EMT testbed of a 100-MW solar PV plus storage grid integration system is simulated. This testbed has full details of plant-level and inverter-level controls. Simulation results confirm the two types of instability phenomena. In addition to EMT simulation studies, we also perturbed the system to obtain measurements for subsystem model identification. The identified model from power command to PLL angle facilitates stability analysis with the plantlevel control included. Both simulation results and the datadriven analysis results demonstrate the two types of plant-level control and PLL interactions.

Besides analysis, two stability enhancement strategies are examined, including slowing down the POI PLL and the inclusion of the additional power PI feedback control. The latter is found to significantly improve stability by offering attenuation.

The findings of this paper and the modeling methods help plant-level control design by avoiding interactions and understanding potential challenges. The IBR power plant considered is the grid following type and findings of this paper are for grid-following IBRs only. For grid-forming IBRs, further investigation is necessary due to their very different control structure and the resulting different dynamic characteristics.



Lingling Fan (Fellow, IEEE) received the B.S. and M.S. degrees in electrical engineering from Southeast University, Nanjing, China, in 1994 and 1997, respectively, and the Ph.D. degree in electrical engineering from West Virginia University, Morgantown, in 2001.

Currently, she is a full professor with the University of South Florida, Tampa, where she has been since 2009. She was a Senior Engineer in the Transmission Asset Management Department, Midwest ISO, St. Paul, MN, form 2001 to 2007, and

an Assistant Professor with North Dakota State University, Fargo, from 2007 to 2009. Her research interests include power systems and power electronics. Dr. Fan serves as Editor-in-Chief for IEEE Electrification Magazine and Associate Editor for IEEE trans. Energy Conversion.



Zhixin Miao (Senior Member, IEEE) received the B.S.E.E. degree from the Huazhong University of Science and Technology, Wuhan, China, in 1992, the M.S.E.E. degree from the Graduate School, Nanjing Automation Research Institute (Nanjing, China) in 1997, and the Ph.D. degree in electrical engineering from West Virginia University, Morgantown, in 2002.

Currently, he is with the University of South Florida (USF), Tampa. Prior to joining USF in 2009, he was with the Transmission Asset Management

Department with Midwest ISO, St. Paul, MN, from 2002 to 2009. His research interests include power system stability, microgrids, and renewable energy. Dr. Miao serves as an associate editor for IEEE trans. Sustainable Energy.



Deepak Ramasubramanian (Senior Member, IEEE) received the M.Tech. degree from the Indian Institute of Technology Delhi, New Delhi, India, in 2013 and Ph.D. degree at Arizona State University, Tempe, AZ, USA in 2017. Deepak is presently a Technical Leader in the Grid Operations and Planning Group at Electric Power Research Institute (EPRI) and leads research projects related to modeling of inverter-based resources for bulk power system analysis.